PLATELETS AND THROMBOPOIESIS

Programmable 3D silk bone marrow niche for platelet generation ex vivo and modeling of megakaryopoiesis pathologies

Christian A. Di Buduo,[1,2] Lindsay S. Wray,[1,2,3] Lorenzo Tozzi,[1,2,3] Alessandro Malara,[1,2] Ying Chen,[3] Chiara E. Ghezzi,[3] Daniel Smoot,[3] Carla Sfara,[4] Antonella Antonelli,[4] Elise Spedden,[5] Giovanna Bruni,[6] Cristian Staii,[5] Luigi De Marco,[7,8] Mauro Magnani,[4] David L. Kaplan,[3] and Alessandra Balduini[1,2,3]

[1]Department of Molecular Medicine, University of Pavia, Pavia, Italy; [2]Biotechnology Research Laboratories, Istituto di Ricovero e Cura a Carattere Scientifico San Matteo Foundation, Pavia, Italy; [3]Department of Biomedical Engineering, Tufts University, Medford, MA; [4]Department of Biomolecular Sciences, Biochemistry and Molecular Biology Section, University of Urbino "Carlo Bo," Urbino, Italy; [5]Department of Physics, Tufts University, Medford, MA; [6]Department of Chemistry, Physical Chemistry Section, University of Pavia, Pavia, Italy; [7]Department of Translational Research, Stem Cells Unit, Istituto di Ricovero e Cura a Carattere Scientifico Centro di Riferimento Oncologico, Aviano, Italy; and [8]Department of Molecular and Experimental Research, The Scripps Research Institute, La Jolla, CA

Key Points

- Natural silk protein sponge and vascular tubes reproduce human bone marrow niche environments for functional platelet generation ex vivo.
- Programmable bioengineered model for the investigation and therapeutic targeting of altered platelet formation.

We present a programmable bioengineered 3-dimensional silk-based bone marrow niche tissue system that successfully mimics the physiology of human bone marrow environment allowing us to manufacture functional human platelets ex vivo. Using stem/progenitor cells, megakaryocyte function and platelet generation were recorded in response to variations in extracellular matrix components, surface topography, stiffness, coculture with endothelial cells, and shear forces. Millions of human platelets were produced and showed to be functional based on multiple activation tests. Using adult hematopoietic progenitor cells our system demonstrated the ability to reproduce key steps of thrombopoiesis, including alterations observed in diseased states. A critical feature of the system is the use of natural silk protein biomaterial allowing us to leverage its biocompatibility, nonthrombogenic features, programmable mechanical properties, and surface binding of cytokines, extracellular matrix components, and endothelial-derived proteins. This in turn offers new opportunities for the study of blood component production ex vivo and provides a superior tissue system for the study of pathologic mechanisms of human platelet production. (*Blood*. 2015;125(14):2254-2264)

Introduction

Bone marrow failure is the result of diseases, trauma, or cancer treatments, leading to a decreased production of blood cells and consequent necessity of blood transfusions.[1] There is a critical need for bioengineering models that are able to reproduce key features of the physiological bone marrow environment to provide mechanistic understanding and control of hematopoiesis, as well as systems for functional blood cell generation and screening of therapeutic compounds ex vivo.[2-5]

Bone marrow microenvironment and "niches," contained in spongy bones, support hematopoietic stem cell self-renewal, as well as differentiation into committed lineages, to support the physiologic homeostasis of blood cells.[6,7] The venous sinusoids are the site of the passage of mature blood cells between the bone marrow compartment and the blood stream. The walls of the sinusoids consist solely of a layer of endothelial cells on a discontinuous basement membrane.[8] Endothelial cells and extracellular matrix (ECM) components are important for the maintenance of correct hematopoiesis.[9-11] In the bone marrow, platelets are generated by megakaryocytes (Mks) that associate with the bone marrow vasculature, where they convert their cytoplasm into proplatelets that protrude through the vascular endothelium and release platelets into the lumen.[12-14]

In this study, we successfully programmed silk protein biomaterial, a biologically derived protein polymer with invaluable properties for tissue engineering,[15] to develop an ex vivo 3-dimensional (3D) tissue model of the bone marrow niche environment in which human Mk function and platelet generation were measured in response to changes in ECM composition, surface topography, stiffness, coculture with endothelial cells, and shear.

Methods

Silk scaffolds fabrication

To explore the possibility to use silk as a scaffold for reproducing the physiologic properties of the basement membrane in vitro, silk solution (1% w/v), produced by degumming *Bombyx mori* silkworm cocoons,[16] containing polyethylene

Submitted August 20, 2014; accepted January 3, 2015. Prepublished online as *Blood* First Edition paper, January 9, 2015; DOI 10.1182/blood-2014-08-595561.

C.A.D.B. and L.S.W. contributed equally to this study.

The online version of this article contains a data supplement.

There is an Inside *Blood* Commentary on this article in this issue.

The publication costs of this article were defrayed in part by page charge payment. Therefore, and solely to indicate this fact, this article is hereby marked "advertisement" in accordance with 18 USC section 1734.

Table 1. Spatial parameters of the surface patterns used

Pattern	Depth (nm ± SD)	Width (nm ± SD)	Roughness (nm ± SD)
None	—	—	3.2 ± 0.5
I	39 ± 5.3	445 ± 33	11.6 ± 1.6
II	64 ± 4.1	1796 ± 173	19.5 ± 1.3
III	465 ± 55	1898 ± 113	156.7 ± 13.8

oxide (PEO) porogen (0.05% w/v; Sigma) was cast on polydimethylsiloxane (PDMS; Dow Corning) molds (45 μL/cm^2 of mold surface area) with different patterns (Table 1) and dried at 22°C for 16 hours.[17] ECM components were added to the silk film, either coated onto the film surface or entrapped within the silk film. The following ECM components were used: 25 μg/mL type I collagen, 100 μg/mL fibrinogen, 25 μg/mL fibronectin, 25 μg/mL type IV collagen, or 25 μg/mL laminin. In some experiments, silk was mixed with ECM components together with 500 ng/mL vascular cell adhesion molecule-1 (VCAM-1) and 500 ng/mL vascular endothelial growth factor (VEGF). To achieve high, medium, and low silk film mechanical properties, samples were water annealed[18] in a vacuum chamber containing 100 mL of water at the bottom of chamber at 60°C for 16 hours, 22°C for 16 hours, or 4°C for 6 hours.

Bone marrow microvasculature was mimicked by preparation of gel-spun microtubes.[19] Briefly, 15% aqueous silk solution was mixed with fibronectin, type IV collagen, and laminin to a final concentration of 25 μg/mL and with 300 ng/mL stromal cell-derived factor (SDF)-1α. In some experiments, the preparation was also mixed with 500 ng/mL VCAM-1 and 500 ng/mL VEGF. Pores were obtained by adding 6% w/v PEO to the silk fibroin to a volume ratio of 10:1 silk:PEO. Functionalized silk tubes were trimmed to ~1.5 cm in length and secured over the blunt end needles within the perfusion bioreactor chamber.

A porous silk sponge was assembled around the tube using a salt-leaching process.[18] Specifically, an 8% aqueous silk solution was dispensed around the tube, and then NaCl particles (~500 μm in diameter) were sifted into the silk solution in a ratio of 1 mL of 8% silk solution to 2 g of NaCl particles. The scaffolds were placed at room temperature for 48 hours and then soaked in distilled water for 48 hours to leach out the NaCl particles.

The supplemental Methods available on the *Blood* Web site provides all technical details.

Results

Silk film surface topography and stiffness direct human megakaryocyte behavior

Porous silk films were fabricated by casting a silk solution onto a PDMS mold with different patterns (Figure 1A; Table 1). We obtained 2- to 5-μm-thick silk films with pores that transcended through the thickness of the films (Figure 1B). As shown in Figure 1C, surface topography significantly affected Mk adhesion compared with nonpatterned silk films.

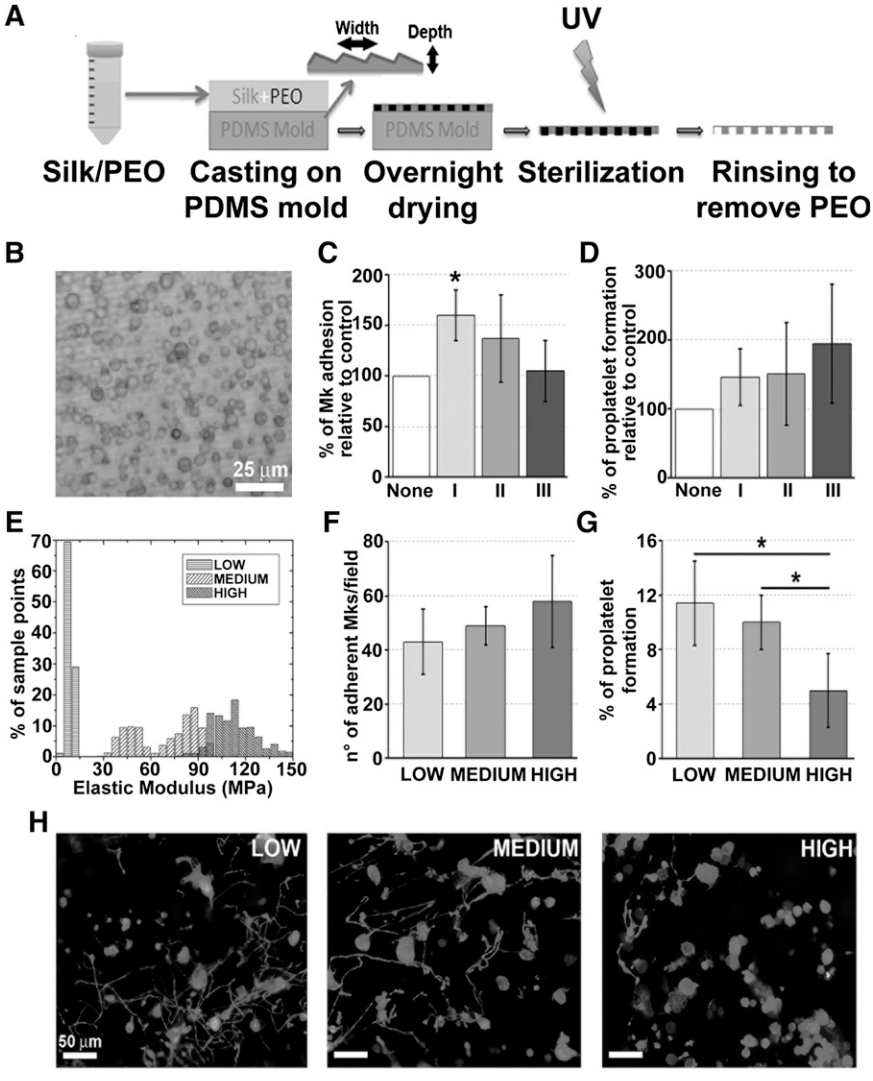

Figure 1. Effect of silk film topography and stiffness on human megakaryocyte adhesion and proplatelet formation. (A) Silk films are prepared by dispensing a silk and PEO solution onto a PDMS mold. The surface of the mold may contain a grating pattern with defined depth and width. When the solution dries, a silk film is formed that contains a dispersion of PEO porogen. The film is finally soaked in phosphate-buffered saline to remove the PEO porogen. (B) Representative light microscopy image of silk film porosity (scale bar = 25 μm). (C-D) Analysis of Mk adhesion and proplatelet formation on silk film with different topography coated with fibrinogen (average ± standard deviatoin [SD], n = 3, *$P < .05$). Results are presented relative to silk film with no pattern. (E) Atomic force microscopy elastic modulus values obtained over hydrated low, medium, and high films. Distributions are displayed as percent of total sample points measured per bin. All samples had a minimum of 300 measurements. (F) There was no significant difference in Mk adhesion between the different stiffness samples (average ± SD, n = 4, P = not significant). (G) The low stiffness samples had similar proplatelet formation compared with the medium stiffness but significantly higher percentage compared with the high stiffness samples (average ± SD, n = 4, *$P < .01$). (H) Representative β1-tubulin staining of Mks cultured on silk films with different stiffness coated with fibrinogen, after a 16-hour incubation. The low stiffness silk films supported long proplatelet extensions and increased silk film stiffness appeared to decreased proplatelet branching (scale bar = 50 μm).

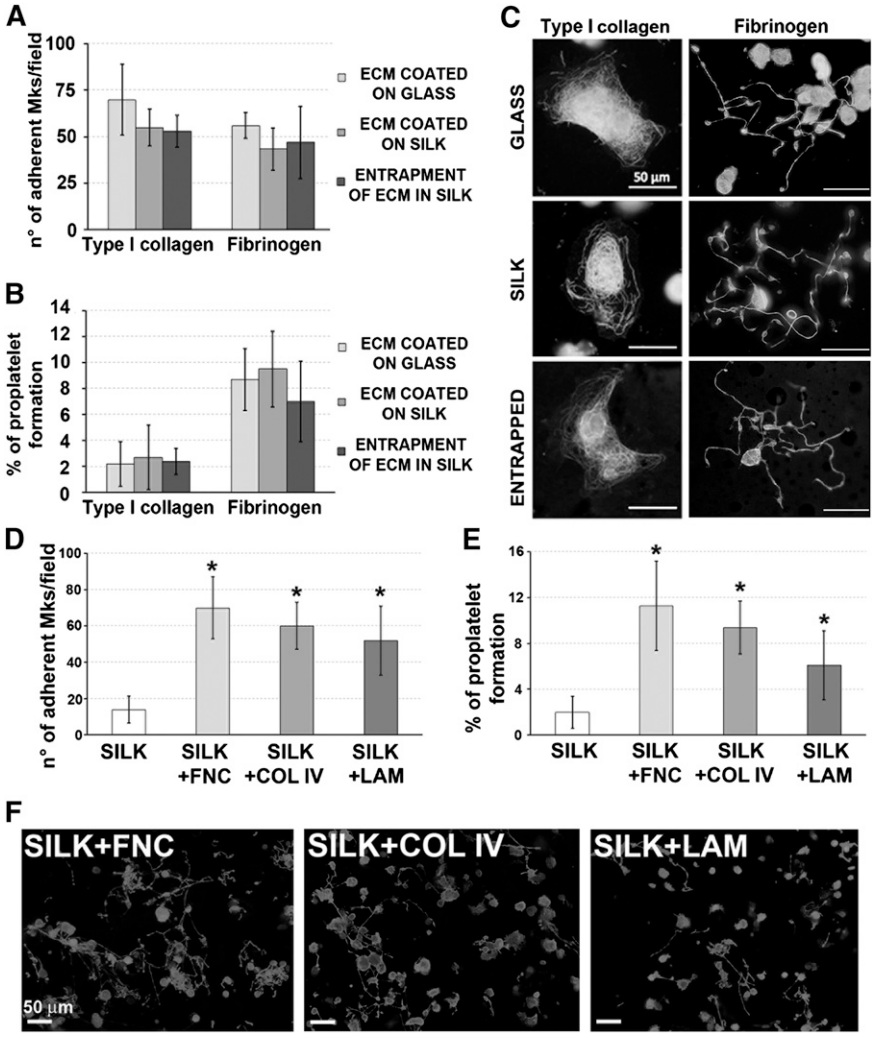

Figure 2. Effect of silk film functionalization on human megakaryocyte adhesion and proplatelet formation. (A-B) Mk adhesion and proplatelet formation on ECM entrapped within silk film followed a similar trend compared with ECM coated on glass coverslip or coated on silk film (average ± SD, n = 4, P = not significant). (C) Representative α-tubulin staining of Mks cultured on coated glass coverslip, coated silk film, or entrapped silk film. Mks were able to sense the proteins entrapped in silk film as they normally spread on type I collagen and form proplatelet on fibrinogen in all tested conditions (scale bar = 50 μm). (D-E) Analysis of silk film functionalization with bone marrow vascular niche ECM components: fibronectin (FNC), type IV collagen (COL IV), and laminin (LAM). Both Mk adhesion and proplatelet formation were not different between the 3 tested ECM components, but significantly higher compared with the nonfunctionalized silk film control only (average ± SD, n = 3, $*P < .05$). (F) Representative β1-tubulin staining of Mks cultured for 16 hours on functionalized silk films shows that proplatelet morphology was almost similar between the 3 tested conditions (scale bar = 50 μm).

Indeed, pattern I displayed the major improvement on Mk adhesion, whereas no significant differences in proplatelet formation were observed (Figure 1D). Therefore, pattern I, was chosen as processing conditions for further characterization. Next, we reproduced different stiffness[20-22] (hereinafter referred as to low, medium, and high protocols) in our system by varying the processing protocols and the elastic modulus was measured via atomic force microscopy nano-indentation (Figure 1E). As shown in Figure 1F, silk film stiffness did not significantly affect Mk adhesion but did affect the percent of Mks that extended proplatelets, with the low and medium stiffness supporting significantly higher percentage of long, branched proplatelets compared with the high stiffness sample (Figure 1G-H). On this basis, medium stiffness was chosen as the optimum condition to maximize Mk function for further characterization.

Silk film ECM component functionalization supports human megakaryocyte development

Silk films were functionalized by surface coating or entrapment with either type collagen I or fibrinogen.[23-26] Regardless of the functionalization method, silk films sustained similar Mk adhesion and proplatelet formation compared with glass coverslips coated with the same molecules (Figure 2A-B). Further, Mk morphology was comparable in all the conditions (Figure 2C). Most importantly, Mks sensed the ECM component entrapped in the silk film. Specifically, sustained spreading and inhibition of proplatelet formation was observed on type I collagen entrapped silk films, whereas proplatelet formation was observed on fibrinogen entrapped films. Silk films were also functionalized with fibronectin, type IV collagen, and laminin that are the most represented ECM components around the bone marrow sinusoids.[27] Functionalization significantly improved both Mk adhesion and proplatelet formation over the silk film only (Figures 2D-F). Overall, these data indicated that ECM components are stable inside silk films and maintain their biological activity on Mk function.

Coculture with endothelial cells increases proplatelet formation and platelet release

Silk films were mounted on plastic transwells. Endothelial primary cells (EPCs) from human cord blood[28] were cultured on the bottom side of the silk films until confluence, and Mks were seeded on the upper side (Figure 3A). Immunofluorescence imaging showed similar endothelial cell cobble-stone morphology on the silk films compared with the glass (Figure 3Bi-Bii) and that cocultures supported both Mk adhesion (Figure 3Biii) and proplatelet formation (Figure 3Biv). Importantly, Mks and endothelial cells remained localized to their respective side, separated by the functionalized porous silk film representing the discontinuous physiologic basement membrane of bone vasculature (Figure 3Bv-vi). EPCs significantly improved Mk adhesion and proplatelet formation with respect to functionalized silk only

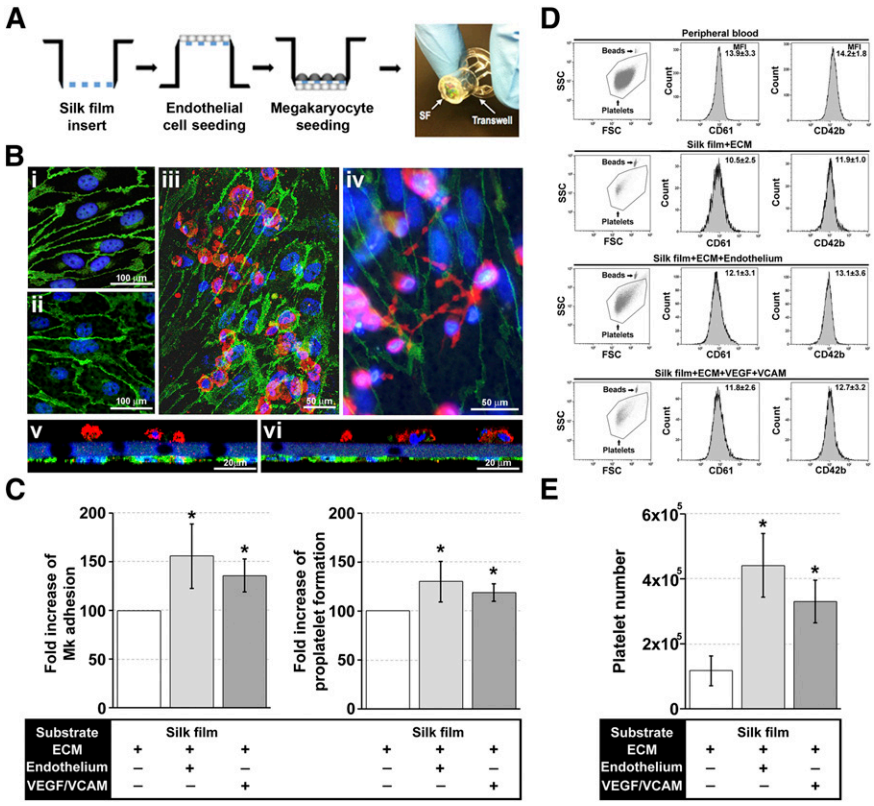

Figure 3. Role of endothelial cells and endothelial-derived molecules in the regulation of platelet formation within the silk film culture system. (A) Schematic of the EPC and Mk seeding procedure for establishment of the silk film model. (B) After 16 hours of culture on the basal side of the silk film membrane, EPCs exhibited the characteristic cobblestone morphology and expression of VE-cadherin on both (Bi) glass coverslip control and (Bii) functionalized silk film (green = VE-cadherin, blue = nuclei, scale bar = 100 μm). (Biii-Biv) Representative fluorescent image of Mk and EPC coculture on the silk film culture system (green = VE-cadherin, red = CD61, blue = nuclei, scale bar = 50 μm). (Bv-Bvi) Representative cross-sectional image of Mk and EPC coculture rendered using confocal microscopy. There was distinct localization of the EPCs (green) on the basal side of the membrane and Mks (red) on the upper side of the membrane (green = VE-cadherin, red = CD61, blue = nuclear, scale bar = 20 μm). Silk films were stained with Hoechst 33258 and visualized in blue. (C) Analysis of Mk adhesion and proplatelet formation on silk film functionalized with ECM components in the presence or not of EPCs or VEGF and VCAM-1 (average ± SD, n = 6, $*P < .05$). (D) $CD61^+$ $CD42b^+$ peripheral blood platelets were used to set the platelet gating protocol. Samples were mixed with counting beads to quantify the number of released platelets. Average ± SD of the mean fluorescence intensity of CD61 and CD42b staining from 6 different experiments is reported (P = not significant). (E) Mks cultured on functionalized silk film in the presence of EPCs or VEGF and VCAM-1 produced a significantly increased number of platelets compared with functionalized silk film only (average ± SD, n = 6, $*P < .01$).

(Figure 3C). Moreover, a similar increase of both adhesion and proplatelet formation was observed by silk functionalization with human recombinant endothelial-specific molecules such as VEGF, known to enhance platelet production by C-X-C chemokine receptor type 4–dependent translocation of Mks to the vascular niche,[29,30] and VCAM-1, which interacts with the very late antigen-4 mediating Mk attachment and localization to vascular niche (Figure 3C).[13,31] Platelet gate and CD61/CD42b fluorescence were set on peripheral blood platelet analysis (Figure 3D).[32-34] Interestingly, Mk/EPCs coculture and VEGF/VCAM-1 inclusion determined a four- and threefold increase, respectively, in platelet production with respect to silk films functionalized with ECM components only (Figure 3E).

Silk tube mimics bone marrow microvasculature and allows platelet flow

To mimic bone marrow microvasculature, we fabricated microtubes[19] functionalized via entrapment of ECM components and SDF-1α as a chemo-attractant. The resulting porous silk microtubes, which exhibited physiologically relevant wall thickness (50 ± 20 μm; Figure 4A), were fitted into a bioreactor chamber. Interestingly, functionalized microtubes supported significantly higher Mk adhesion with respect to nonfunctionalized silk microtubes (supplemental Figure 1). The biocompatible and nonthrombogenic properties of microtubes were demonstrated by perfusion of whole peripheral blood or isolated peripheral blood platelets into the silk microtubes at a physiologic shear rate of 60 s^{-1} (Figure 4B).[35,36] As shown in Figure 4C, complete blood counts, before and after perfusion, were almost comparable. Moreover, on passage through the functionalized microtubes, platelets remained quiescent and maintained their capability of responding to physiological stimuli from adenosine diphosphate (ADP) or thrombin (Figure 4D). No signs of clot formation were observed (Figure 4E).

Silk sponge mimics the 3D structure of the bone marrow environment and supports platelet formation

To mimic the 3D spongy architecture that surrounds the marrow vasculature, we assembled a silk sponge around the functionalized silk microtubes and analyzed its properties in supporting Mk function (Figure 5A). Scanning electron microscopy (SEM) and immunofluorescence confocal microscopy showed that the silk sponge consisted of interconnected pores ~100 to 500 μm in diameter (Figures 5B-Ci). A total of 2.5×10^5 mature cord blood-derived Mks were seeded into the system. Human $CD61^+$ Mks not extending proplatelets could be observed 30 minutes after seeding as round and homogeneously distributed cells in the scaffold (Figure 5Cii). Longer incubation revealed changes in Mk localization and morphology. Specifically, after 16 hours, Mks migrated toward the vascular tube and adhered to the outer wall (Figure 5Ciii). Furthermore, proplatelet-forming Mks distributed along the external wall of the microtubes (Figure 5Civ), and platelet tips protruding into the microtube lumen could be identified (Figure 5Cv). Finally, after 24 hours, whole branched proplatelets were extended into the lumen to release platelets (Figure 5Cvi). Similar morphological changes were further observed by SEM imaging of parallel samples (Figure 5Di-vi). Interestingly, in the absence of SDF-1α, fewer Mks reached the microtube surface, with proplatelet formation occurring mainly within sponge pores, thus underlying the role of the chemo-attractant in regulating Mk migration (supplemental Figure 2A-B).

Human megakaryocytes release functional platelets into the perfused vascular silk tube lumen

Blood flow was mimicked by perfusing culture media into the silk microtube at a shear rate of 60 s^{-1}. The flow through of the vascular microtube was collected into a gas-permeable collection bag

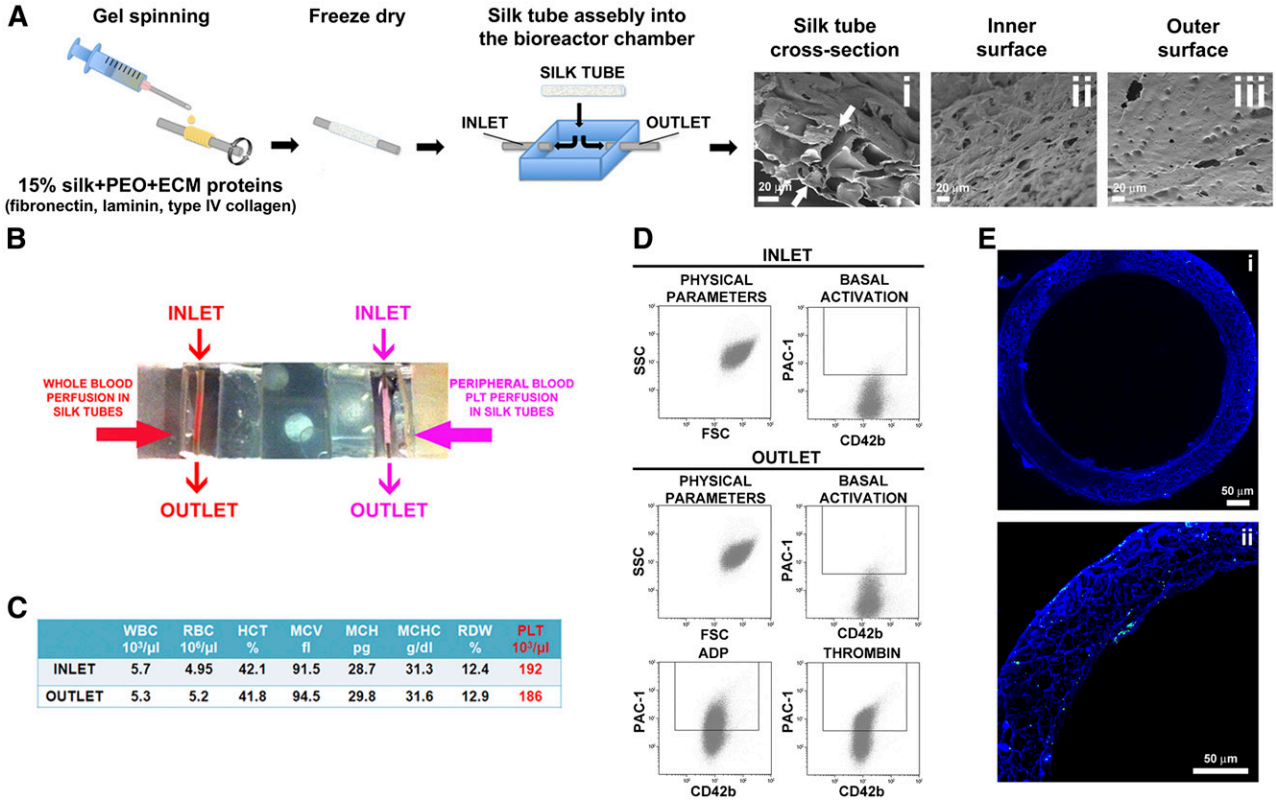

C

	WBC $10^3/\mu l$	RBC $10^6/\mu l$	HCT %	MCV fl	MCH pg	MCHC g/dl	RDW %	PLT $10^3/\mu l$
INLET	5.7	4.95	42.1	91.5	28.7	31.3	12.4	192
OUTLET	5.3	5.2	41.8	94.5	29.8	31.6	12.9	186

Figure 4. Silk microtube fabrication and analysis of their ability to support platelet perfusion. (A) Silk microtubes are prepared by gel spinning aqueous silk solutions containing PEO porogen around a wire and functionalized via entrapment of ECM components. Resulting microtubes are freeze dried, removed from the wire, and soaked in water to leach out the PEO porogen. The resulting porous silk microtubes are fitted into the bioreactor chamber. (Ai) SEM cross sections of a silk microtube: microtube wall thickness was 50 ± 20 μm, with microtube wall pores diameter of 22 ± 4 μm to allow proplatelet elongation (scale bar = 20 μm). Arrows indicate silk microtubes borders. (Aii-Aiii) SEM images show pores on both the inner and outer surfaces of the silk microtubes, respectively. The inner and outer microtube wall pores diameter was 6 ± 2 μm (scale bars = 20 μm). (B) Whole blood (red) or peripheral blood platelets suspended in culture medium (pink) were perfused into functionalized silk microtubes. (C) Representative analysis of whole blood cells of 1 sample before (inlet) or after (outlet) perfusion. WBC, white blood cells; RBC, red blood cells; HCT, hematocrit; MCV, mean corpuscular volume; MCH, mean corpuscular hemoglobin; MCHC, mean corpuscular hemoglobin concentration; RDW, red blood cell distribution width; PLT, platelet. (D) Representative flow cytometry analysis of peripheral blood platelet basal activation before and after perfusion into silk microtube. Activation with ADP and thrombin demonstrated increased PAC-1 binding, indicating normal $CD42b^+$ platelet functionality after the passage through the silk microtube lumen. (E) Confocal microscopy analysis of $CD61^+$ platelet distribution within microtube lumen after passage of whole blood (green = CD61; blue = nuclei; scale bar = 50 μm). Silk fibroin microtubes were stained with Hoechst 33258 and visualized in blue.

containing acid citrate dextrose (ACD) as anticoagulant (Figure 6A). Collected platelets were double stained with anti-CD61 and anti-CD42b antibodies and exhibited similar physical parameters as human peripheral blood platelets, as determined by flow cytometry analysis (Figure 6A). The mean number of $CD61^+CD42b^+$ collected platelets was $1.4 \pm 0.6 \times 10^6$ per 3D tissue perfusion system and linearly increased with the use of multiple bioreactors in parallel (Figure 6A). Moreover, perfusion with erythrocytes suspended in culture medium at 5% of hematocrit did not enhance platelet production compared with media only (supplemental Figure 3). Ex vivo produced platelets morphology, characterized by light microscopy and β1-tubulin immunofluorescence staining, showed all the typical stages of platelet shedding: large cytoplasmic fragments resembling preplatelet intermediates (>4 μm diameter), dumbbell-shaped platelets, and standard disc-shaped platelet (2-4 μm diameter; Figures 6Bi-v). β1-tubulin was mainly distributed at platelet perimeter into the typical platelet microtubule coil (Figure 6Biv-v). Platelet ultrastructure, imaged by transmission electron microscopy, showed the presence of physiological α- and dense-granules (Figure 6Bvi). Parallel flow cytometry analysis of collected platelets, in the presence of calcein-AM, gave a demonstration that almost all analyzed particles were live cells. Importantly, collected platelets kept in transfusional bags, at room temperature with constant agitation, were still alive up to 4 days from collection (data not shown).

Ex vivo produced platelets are functional and can contribute to clot formation

We proceeded to analyze the functionality of ex vivo-produced platelets. Actin staining demonstrated no relevant cytoskeleton organization in resting platelets (Figure 6Ci), whereas, after seeding onto immobilized type I collagen, platelets spread by assembling actin stress fibers (Figure 6Cii-iv). To test platelet functionality in a condition closely mimicking vessel injury, we took advantage of a well-characterized flow chamber system, widely used to study platelet functions.[37,38] For this experiment, Mks were stained with 0.5 μM carboxyfluorescein diacetate succinimidyl ester (CFSE) cell staining dye, before being seeded into the silk-based system. $CFSE^+$ produced platelets were resuspended, to a final concentration of 4×10^6/mL, in Tyrode's buffer containing 100 μg/mL von Willebrand factor and perfused over immobilized type I collagen at a shear rate of 1000 s^{-1}.[39] We observed platelet arrest and adhesion onto the substrate with formation of small platelet aggregates, thus suggesting their ability to promote thrombus formation (Figure 6Cv). This function was further confirmed by a flow cytometry-based platelet aggregation assay,[40] in which collected platelets were

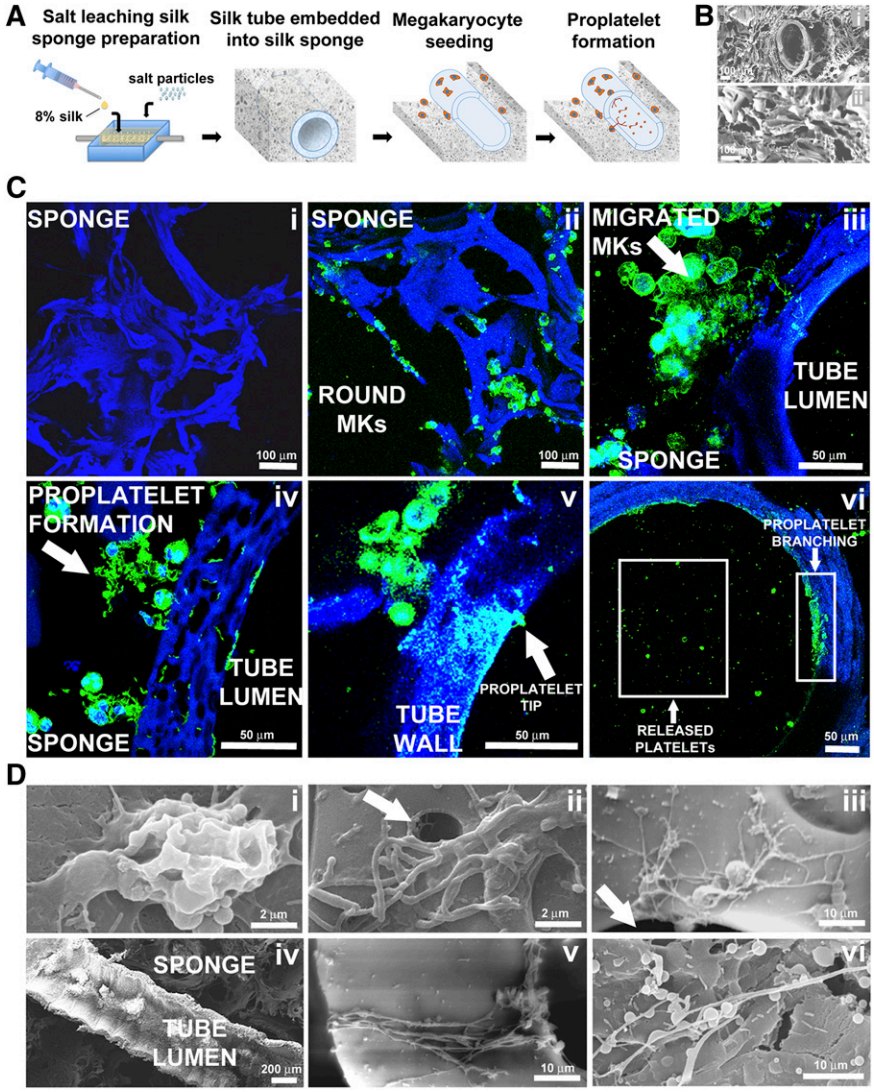

Figure 5. Silk microtube assembly and sponge preparation into the bioreactor chamber and analysis of platelet production within this system. (A) Aqueous silk is dispensed into the chamber around the microtube and salt particles are added. After leaching out the salt, the resulting porous silk sponge is trimmed and sterilized. After seeding into the silk sponge, Mks migrate toward the microtube, adhere, and extend proplatelets through the microtube wall to release platelets into the microtube lumen. (Bi) SEM image showing a silk microtube embedded into the silk sponge (scale bar = 100 μm). (Bii) SEM image showing the porous morphology of silk sponge (scale bar = 100 μm). (C) Confocal microscopy analysis of different steps of Mks behavior within the silk microtube-sponge tissue system. (Ci) Silk sponge before Mks seeding (scale bar = 100 μm). (Cii) Mature Mks immediately after seeding into the silk sponge (green = CD61; blue = nuclei; scale bar = 100 μm). (Ciii) Migrated Mks in close contact with the microtube wall (green = CD61; blue = nuclei; scale bar = 50 μm). (Civ) Mks forming proplatelet on adhesion to the microtube wall (green = CD61; blue = nuclei; scale bar = 50 μm). (Cv) Mk extending proplatelets through the silk microtube wall. Arrow indicates proplatelet branch elongation through microtube wall with proplatelet tip protruding into the microtube lumen (green = CD61; blue = nuclei; scale bar = 50 μm). (Cvi) Boxes highlight proplatelet branches detectable along the inner wall of the silk microtube and platelets released into the microtube lumen (green = CD61; blue = nuclei; scale bar = 50 μm). For all immunofluorescence analysis, silk fibroin 3D scaffolds were stained with Hoechst 33258 and visualized in blue. (D) SEM imaging of different steps of Mks behavior within the silk microtube-sponge tissue system. (Di) Mature Mks adhesion on silk microtube outer wall (scale bar = 2 μm). (Dii-Diii) Migrated Mks forming proplatelet on adhesion to the microtube wall (scale bar = 2 and 10 μm). Arrows indicate silk pores that allow proplatelet elongation inside microtube lumen. (Div) Longitudinal section of silk microtube-sponge tissue system (scale bar = 200 μm). (Dv) Mk extending proplatelets through silk microtube wall (scale bar = 10 μm). (Dvi) Proplatelet branch stemming inside microtube lumen and released platelets (scale bar = 10 μm).

split and single stained with 2 different antibodies: anti-CD31 and anti-CD42b. On union of both platelets populations and activation, we observed the appearance of a double-colored population of aggregated platelets compared with the unactivated control (Figure 6D). Platelet function was finally assessed by the study of ex vivo-produced platelets participation to clot formation in vitro.[41,42] $CFSE^+$ platelets from our tissue system were mixed with peripheral blood platelet stained with CellTracker Deep Red Dye in Tyrode's buffer containing 1 mg/mL fibrinogen and 1 U/mL thrombin. As shown in Figure 6Ei, $CFSE^+$ platelets were distributed homogeneously within the sample. Importantly, peripheral blood (red) and ex vivo-produced platelets (green) were shown to actively interact based on the appearance of overlapping staining (yellow), thus demonstrating the contribution of the latter to clot formation (Figure 6Eii).

Silk vascular tubes can be coated with a confluent endothelium or functionalized with endothelial cell-derived molecules

To further mimic the composition of the vascular niche, human dermal microvascular endothelial cells (HMVEC-d) or EPCs were cultured within the silk microtube lumen before seeding Mks into the silk sponge (Figure 7A).[43,44] Endothelial cells formed a confluent layer covering the inner wall of the silk microtubes with the characteristic cobblestone morphology and VE-cadherin staining (Figure 7Bi-ii). Endothelialized vascular microtubes exhibited a significant increase in the number of collected platelets compared with nonendothelialized silk vascular microtubes (Figure 7C). No differences were observed between the 2 endothelial cell sources (data not shown). Interestingly, silk functionalization with VEGF and VCAM-1, recapitulated the increase in platelet production observed in the presence of endothelium (Figure 7C).

Platelet functionality was determined by flow cytometry analysis of increased PAC-1 binding to the activated integrin $\alpha_{IIb}\beta_3$, on physiologic stimulation with both weak (ie, epinephrine and ADP) and strong (ie, thrombin) agonists, with respect to resting conditions (supplemental Figure 4A). No differences were observed between the presence and absence of endothelial cells (supplemental Figure 4B).

Analysis of ex vivo platelet production from human megakaryocytes derived from adult hematopoietic progenitor cells

We finally investigated how Mks derived from peripheral blood progenitors of healthy subjects and patients with primary myelofibrosis behaved within the system. Time course analysis revealed similar Mk

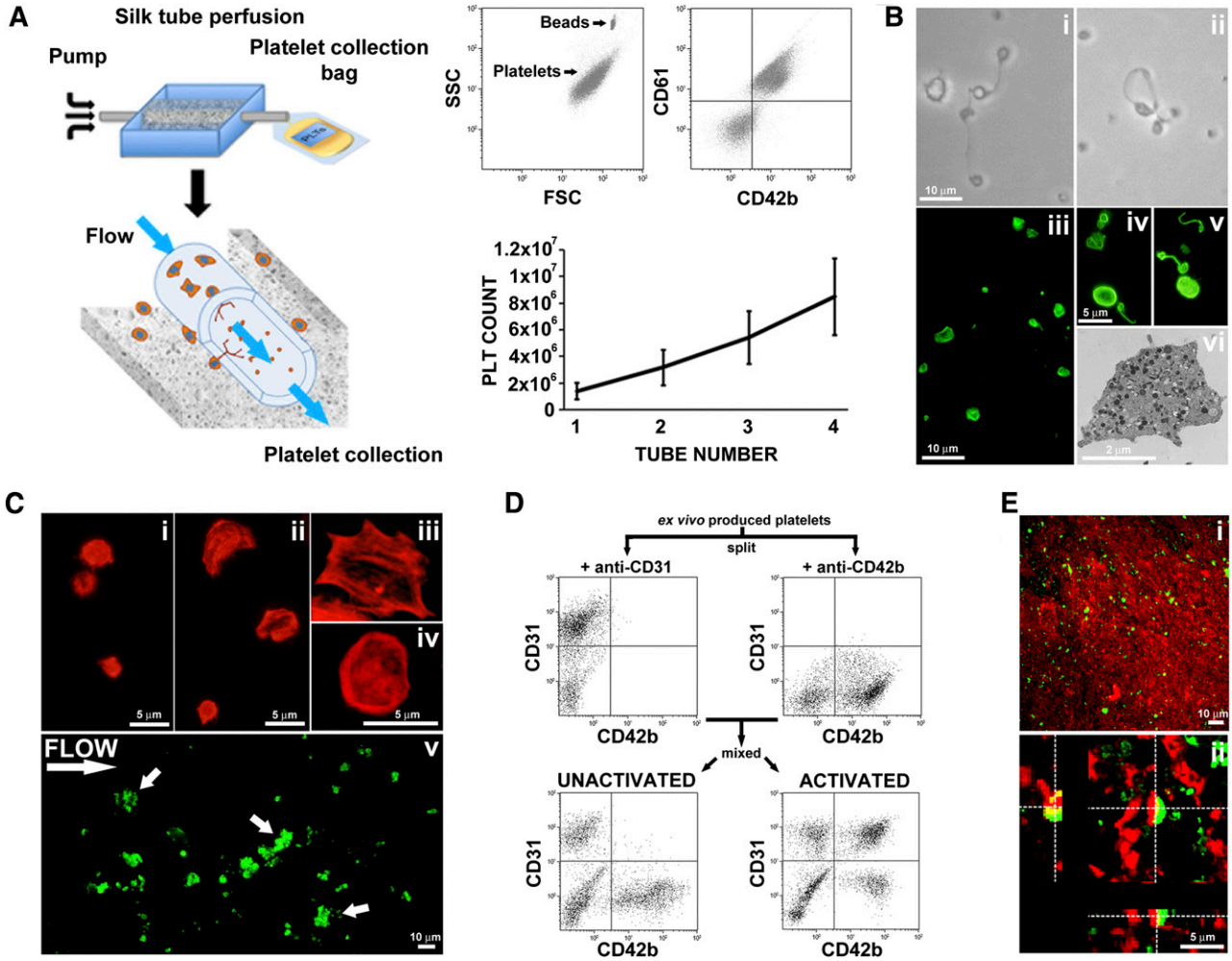

Figure 6. Analysis of ex vivo produced platelets morphology and functionality. (A) Silk microtubes are perfused with culture media for 6 hours, and released platelets are collected into gas-permeable bags. Samples are mixed with counting beads to quantify the number of platelets that are identified as $CD61^+CD42b^+$ events. A maximum of 4 different silk microtubes have been perfused concurrently. The graph shows the absolute number of platelets released per microtube embedded in the silk sponge containing 2.5×10^5 Mks. (B) Analysis of platelet morphology. (Bi-Bii) Light microscopy analysis shows preplatelets, dumbbell-shaped platelets, and disc-shaped platelet (scale bar = 10 μm). (Biii) Immunofluorescence staining of β1-tubulin (green) (scale bar = 10 μm). (Biv-Bv) Magnification highlights the microtubule coil typically showed by resting platelets (scale bar = 5 μm). (Bvi) Transmission electron microscopy analysis of ex vivo produced platelets ultrastructure (scale bar = 2 μm). (C) Analysis of platelet adhesion on type I collagen. (Ci) Tetramethylrhodamine isothiocyanate-phalloidin staining of resting platelets (scale bar = 5 μm). (Cii) After adhesion on type I collagen platelets spread and formed filopodia/lamellipodia (scale bar = 5 μm). (Ciii-Civ) Magnification highlights actin cytoskeleton reorganization with evident stress fibers assembly (scale bar = 5 μm). (Cv) $CFSE^+$ platelets were suspended into Tyrode's buffer containing von Willebrand factor and perfused over immobilized type I collagen at shear rate of 1000 s^{-1}. Image shows a representative filed demonstrating platelet adhesion. Arrows indicate formation of platelet aggregates (scale bar = 10 μm). (D) Aggregation capacity was further measured by flow cytometry after stimulation with thrombin, ADP, and epinephrine. Platelets were separately labeled with CD31 or CD42b (left and right top, respectively), and then mixed 1:1, before being stimulated (bottom right) or not (bottom left) with the cocktail of agonists. (E) Analysis of ex vivo produced platelets participation to clot formation. (Ei) Ex vivo produced $CFSE^+$ platelets were mixed with peripheral blood platelet stained with CellTracker Deep Red Dye. Clot formation was favored by addition of thrombin and visualized by confocal microscopy (scale bar = 10 μm). (Eii) Cross-sectional analysis of z-stack of the clot demonstrating that ex vivo produced platelets (green) actively interacted with in vivo derived platelets (red) with appearance of a juxtaposed signal (yellow) (scale bar = 5 μm).

behavior to that observed with cord-blood derived Mks, with $CD61^+$ round Mks homogeneously distributed within the sponge at the beginning of the experiment and proplatelet extension across the tube lumen after a 24-hour incubation (Figure 8Ai-vi). However, patient 1-derived Mks displayed higher branched proplatelets, whereas patient 2 had fewer and shorter proplatelet shafts than healthy control (Figure 8Aiv-vi). This evidence was paralleled by an increase in $CD61^+CD42b^+$ platelets release by patient 1 Mks and a reduced number of collected platelets from patient 2 with respect to healthy controls (Figure 8B). Results obtained were further supported by the comparison of ex vivo and in vivo platelet count (Figure 8C). Interestingly, patient 1, who showed the higher thrombopoietic potential in our 3D system, had an history of high peripheral blood platelet count, whereas patient 2, characterized by a reduced ex vivo platelet biogenesis, presented a low platelet count compared with physiologic range. These data are consistent with our previous finding demonstrating a significant correlation between in vivo platelet count and in vitro proplatelet formation from patients with myeloproliferative neoplasms.[45]

Discussion

Silk protein can be transformed into a wide range of material formats that can be integrated to reproduce a niche-like bone marrow microenvironment. Through a complete redesign of our initial model,[2] we engineered a 3D bone marrow model made of porous silk to fully

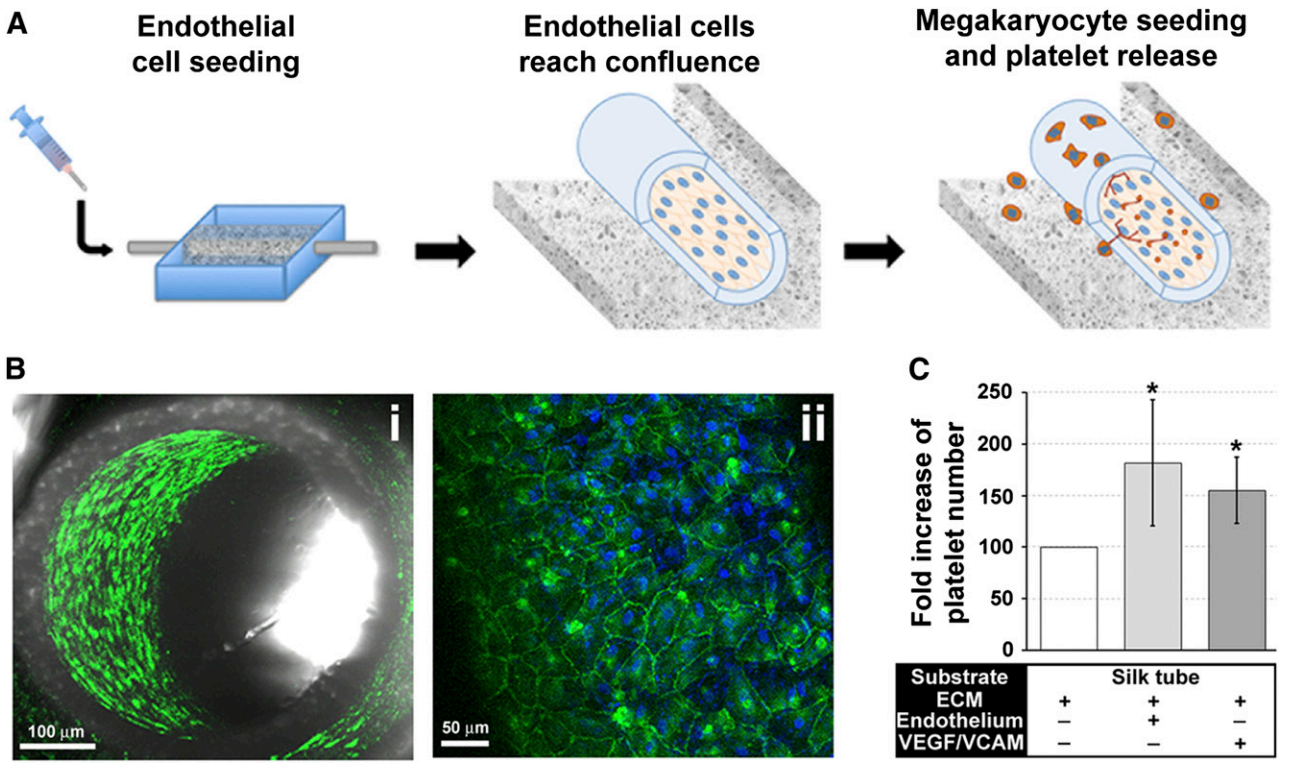

Figure 7. Adding complexity to the system: endothelial and endothelial-derived molecules promote platelet collection. (A) The silk microtube lumen supports a confluent monolayer of human endothelial cells. (Bi) Confocal microscopy images of confluent HMVEC-d into the silk microtube lumen (green = VE-cadherin; scale bar = 100 μM). (Bii) Magnification of HMVEC-d seeded into silk microtube lumen (green = VE-cadherin; blue = nuclei; scale bar = 50 μM). (C) Statistical analysis of collected platelets after perfusion of silk microtubes in presence of endothelium or functionalized with VEGF and VCAM-1 with respect to silk microtube functionalized with ECM components only (average ± SD, n = 5, $*P < .05$).

recreate the physiology of human bone marrow niche environment. Our new system is capable of successfully generating functional platelets ex vivo, with endothelial cells cocultures significantly increasing the numbers of released platelets.

Because of this novel system, we identified and exploited numerous unique properties of silk biomaterial for physiologically relevant bone marrow modeling and platelet production. First, we modeled silk to control topography and stiffness, both features that have been shown to affect Mk adhesion and proplatelet formation.[21,46] Cells in vivo are exposed to diverse topographies, depending on tissue structure and ECM composition that may exert a major impact on their function.[47-49] We demonstrated that lower surface roughness results in a better outcome in terms of Mk adhesion, consistent with the notion that perivascular space is mainly a continuous surface.[22] In contrast, Mk adhesion was unaffected by substrate stiffness whereas proplatelet formation and branching decreased on stiffer substrates. The rigidity of the human basement membrane located in the perivascular space is still unclear.[22] However, these results are consistent with the evidence that soft substrates better sustain platelet production.[21] Second, we functionalized the silk by either surface coating or entrapment of ECM components. The advantage of entrapping the ECM components within the silk film is that silk has been shown to stabilize bioactive molecules at physiologic conditions without loss of bioactivity.[50] Accordingly, there was no difference between Mk adhesion and proplatelet formation on functionalized silk films that had been coated or that had the ECM protein entrapped within the film as Mks were able to sense the ECM component entrapped in the silk film and behave consequently. Then, we cultured endothelial cells with Mks under experimental settings where the 2 cell types were physically separated by functionalized silk. Mks/endothelial cells coculture has shown that chemokines released by the endothelial cells contribute to Mk maturation, Mk localization to the vascular niche, and increased platelet production.[13] Additionally, Mk adhesion to endothelial cells increases Mk proliferation and maturation.[12,31,51] We confirmed the importance of Mks and endothelial cells coculture by measuring a significant increase in platelet production in the coculture conditions compared with the Mk-only cultures, suggesting that the tunable features of the silk film model, namely ECM entrapment, surface topography, and stiffness, optimized with the concomitant presence of endothelial cells can support platelet production and release ex vivo. In addition, we observed that silk functionalization with VEGF and VCAM-1, recapitulated the increase in platelet production observed in the presence of endothelium, thus suggesting that endothelial cells could be replaced by recombinant endothelial derived molecules.

The insights gained with the basement membrane model guided us in the assembly of the silk-sponge based bone marrow system closely mimicking the 3D bone marrow structure and composition with great improvement with respect to our previous model.[2] Specifically, a silk sponge mimicked the 3D environment where hematopoiesis takes place; entrapment of ECM components and SDF-1α in silk microtube wall allowed us to avoid the use of gels, thus obtaining a chemoattractive thin basement membrane-like layer of silk. Finally, blood flow was mimicked by perfusion of culture media at a shear rate of 60 s^{-1} that has been described to be exerted into mouse bone marrow sinusoids and to promote platelet production by human Mks.[35,36] Importantly, media perfusion improved the yield of released platelets

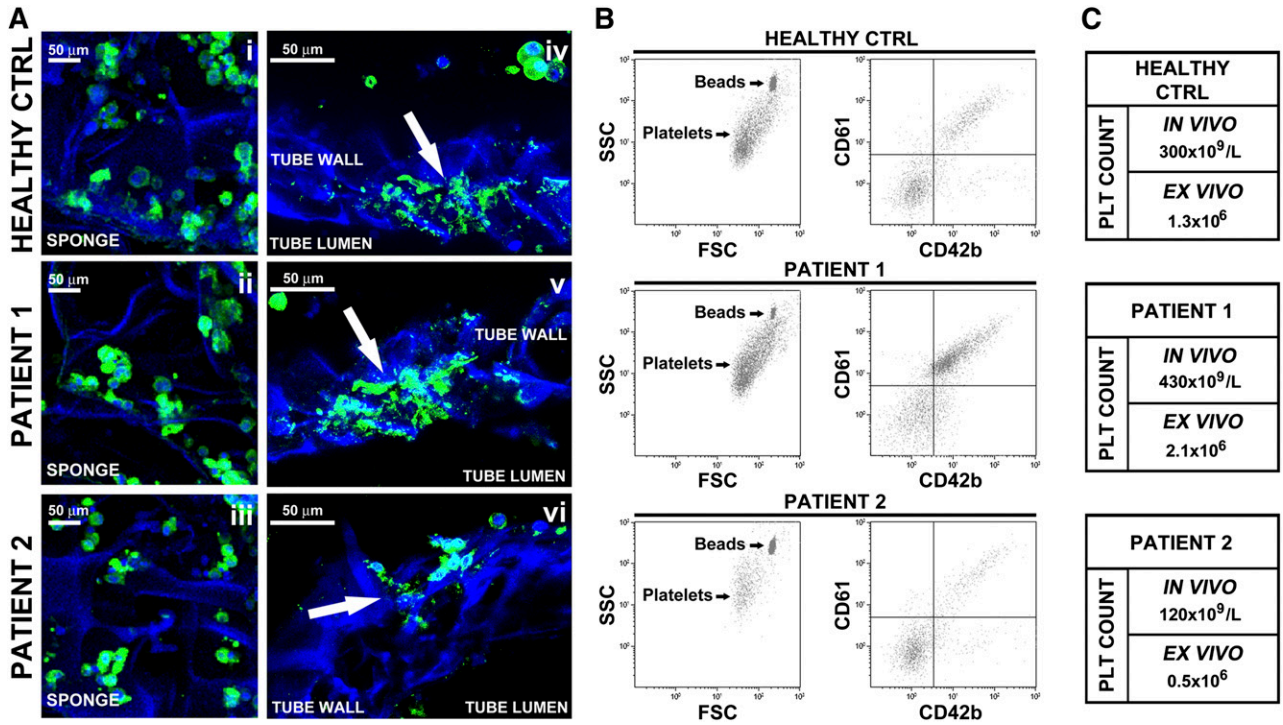

Figure 8. Analysis of ex vivo platelet release by Mks differentiated from adult human peripheral blood hematopoietic progenitors. (A) Confocal microscopy imaging of Mks from 1 healthy control and 2 patients within the silk-based bone marrow system. (Ai-Aiii) Imaging of mature Mks immediately after seeding into the silk sponge (green = CD61; blue = nuclei; scale bar = 50 μm). (Aiv-Avi) Mks forming proplatelet through the silk microtube wall (green = CD61; blue = nuclei; scale bar = 50 μm). Arrows indicate proplatelet branching and elongation. Silk fibroin 3D scaffolds were stained with Hoechst 33258 and visualized in blue. (B) Flow cytometry analysis of ex vivo-produced platelets. Samples were mixed with counting beads to quantify the number of $CD61^{+}CD42b^{+}$ platelets. (C) Comparison of platelet count between in vivo and ex vivo quantified numbers.

through the 3D silk tissue with respect to static condition, whereas perfusion with reconstituted red blood cells did not impact on platelet production. However, the perfusion of red blood cells represents an important step to strengthen our strategy in reproducing the physiological blood flow of the vascular bone marrow niche and in the future will offer the unique possibility to modulate oxygen tension inside the system.[52,53] Interestingly, further increase in the number of collected platelets was obtained by the presence of endothelial cells within the tube lumen or silk functionalization with endothelium-derived recombinant molecules, thus indicating that for future scaled-up production we will be able to avoid the use of endothelial cells by mixing silk with these or others specific recombinant molecules of endothelial origin able to promote Mk function.

Overall, the combination of the unique features of the present model together with the modular bioreactor setup led to a threefold increase in total platelet yield compared with our previous system.[2] Thus, the more closely we mimic the bone marrow environment the greater number of platelets are collected. Even though the number of platelets per Mk may be considered still low with respect to estimated values in vivo,[54] making this a major point to be investigated, we believe that being able to produce sufficient platelets suitable for further analysis is a fundamental advantage toward understanding the mechanisms of platelet production in healthy and disease conditions. To this regard, the improvements of this new system allowed us to better characterize ex vivo produced platelet morphology by different microscopy approaches and platelet functionality by a variety of in vitro assays demonstrating the ability to aggregate and form thrombi. Most importantly, we demonstrated that similar platelet production can be obtained by exploiting our system with hematopoietic progenitor cells from different sources, including patient-derived Mks. Interestingly, a significant correlation among proplatelet branching along the silk vascular tube, the extent of platelet release ex vivo and in vivo platelet count was observed when Mks, derived from patients with primary myelofibrosis,[45] were seeded in the bone marrow model. This in turn leads us to believe that our system will provide unique opportunities for clinical applications.

Different 3D tools have been described thus far in the attempt of supporting thrombopoiesis by both mouse and human Mks differentiated from either hematopoietic progenitors or the promising induced pluripotent stem cells.[4,5,55-59] Despite the usefulness for the advancement in providing systems for platelet production, all these models did not reproduce the complex microenvironment where megakaryopoiesis physiologically takes place. In this regard, a fundamental advantage of our model is its ability to provide the first ex vivo tissue system able to reproduce the 3D structure of the bone marrow niche, in combination with ECM components and physiologic shear rate, for the study of Mk function and platelet formation. Going forward with this system should provide a platform for studying mechanisms of megakaryopoiesis for further elucidation of the processes that regulate platelet production. This insight will in turn shed light on megakaryopoiesis-related disease progression. Patient-derived Mks and endothelial cells, which can be derived from several depots throughout the body, can be cultured in this model and used to design patient-specific drug administration regimes. Additionally, ex vivo generated platelets could be used as a source of growth factors for wound healing in regenerative medicine, including healing of recalcitrant ulcers and burns, and stimulation of osseous tissue regeneration in dentistry and maxillofacial plastic surgery.[60] Last, this 3D bone marrow tissue perfusion system provides a versatile tool for studying hematopoiesis ex vivo offering additional opportunities in elucidating fundamental biological mechanisms of hematopoiesis and for clinical application in

diagnosing and treating disease while avoiding the need for animal models.

Acknowledgments

The authors thank Centro Grandi Strumenti of the University of Pavia, Dr Patrizia Vaghi and Dr Vittorio Necchi for technical assistance with confocal and transmission electron microscopy, Dr Gianluca Viarengo, Dr Laura Vanelli, and Prof Federica Meloni for technical assistance with the flow cytometry analysis, Dr Cesare Perotti and Dr Laura Salvaneschi for supplying human cord and peripheral blood, Dr Mario Mazzucato and Dr Monica Battiston for technical assistance in the study of platelet adhesion under flow, Dr Giovanni Barosi and Dr Vittorio Rosti for supplying patients' peripheral blood, and Prof Joseph Italiano for providing β1-tubulin antibody.

This work was supported by the Cariplo Foundation (2010-0807), National Institutes of Health, National Institute of Biomedical Imaging and Bioengeneering (grant EB016041-01), the Italian Ministry of Health (grants RF-2009-1550218 and RF-2010-2316198), the Italian Ministry of University and Research, Fondo per gli Investimenti della Ricerca di Base (RBFR1299KO), and by a grant from the Associazione Italiana per la Ricerca sul Cancro (AIRC, Milano) "Special Program Molecular Clinical Oncology 5x1000" to AIRC-Gruppo Italiano Malattie Mieloproliferative (AGIMM).

The funders had no role in study design, data collection and analysis, decision to publish, or preparation of the manuscript.

Authorship

Contribution: A.B. conceived the idea, supervised the project, and wrote the manuscript; C.A.D.B., L.S.W., L.T., and A.M. designed and performed the experiments, analyzed the data, and wrote the manuscript; Y.C., C.E.G., D.S., C.S., A.A., E.S., and G.B. performed the experiments and edited the manuscript; and C.S., L.D.M., M.M., and D.L.K. analyzed the data and edited the manuscript.

Conflict-of-interest disclosure: The authors declare no competing financial interests.

Correspondence: Alessandra Balduini, Department of Biomedical Engineering, Tufts University, 4 Colby St, Medford, MA 02155; e-mail: alessandra.balduini@tufts.edu; or David L. Kaplan, Department of Biomedical Engineering, Tufts University, 4 Colby St, Medford, MA 02155; e-mail: david.kaplan@tufts.edu.

References

1. DeZern AE, Sekeres MA. The challenging world of cytopenias: distinguishing myelodysplastic syndromes from other disorders of marrow failure. *Oncologist.* 2014;19(7):735-745.
2. Pallotta I, Lovett M, Kaplan DL, Balduini A. Three-dimensional system for the in vitro study of megakaryocytes and functional platelet production using silk-based vascular tubes. *Tissue Eng Part C Methods.* 2011;17(12):1223-1232.
3. Torisawa YS, Spina CS, Mammoto T, et al. Bone marrow-on-a-chip replicates hematopoietic niche physiology in vitro. *Nat Methods.* 2014;11(6):663-669.
4. Nakagawa Y, Nakamura S, Nakajima M, et al. Two differential flows in a bioreactor promoted platelet generation from human pluripotent stem cell-derived megakaryocytes. *Exp Hematol.* 2013;41(8):742-748.
5. Thon JN, Mazutis L, Wu S, et al. Platelet bioreactor-on-a-chip [published online ahead of print July 21, 2014. *Blood*., doi:10.1182/blood-2014-05-574913.
6. Morrison SJ, Scadden DT. The bone marrow niche for haematopoietic stem cells. *Nature.* 2014;505(7483):327-334.
7. Wang LD, Wagers AJ. Dynamic niches in the origination and differentiation of haematopoietic stem cells. *Nat Rev Mol Cell Biol.* 2011;12(10):643-655.
8. Inoue S, Osmond DG. Basement membrane of mouse bone marrow sinusoids shows distinctive structure and proteoglycan composition: a high resolution ultrastructural study. *Anat Rec.* 2001;264(3):294-304.
9. Ohta M, Sakai T, Saga Y, Aizawa S, Saito M. Suppression of hematopoietic activity in tenascin-C-deficient mice. *Blood.* 1998;91(11):4074-4083.
10. Jacenko O, Roberts DW, Campbell MR, McManus PM, Gress CJ, Tao Z. Linking hematopoiesis to endochondral skeletogenesis through analysis of mice transgenic for collagen X. *Am J Pathol.* 2002;160(6):2019-2034.
11. Winkler IG, Barbier V, Nowlan B, et al. Vascular niche E-selectin regulates hematopoietic stem cell dormancy, self renewal and chemoresistance. *Nat Med.* 2012;18(11):1651-1657.
12. Rafii S, Shapiro F, Pettengell R, et al. Human bone marrow microvascular endothelial cells support long-term proliferation and differentiation of myeloid and megakaryocytic progenitors. *Blood.* 1995;86(9):3353-3363.
13. Avecilla ST, Hattori K, Heissig B, et al. Chemokine-mediated interaction of hematopoietic progenitors with the bone marrow vascular niche is required for thrombopoiesis. *Nat Med.* 2004;10(1):64-71.
14. Junt T, Schulze H, Chen Z, et al. Dynamic visualization of thrombopoiesis within bone marrow. *Science.* 2007;317(5845):1767-1770.
15. Vepari C, Kaplan DL. Silk as a Biomaterial. *Prog Polym Sci.* 2007;32(8-9):991-1007.
16. Lovett M, Cannizzaro C, Daheron L, Messmer B, Vunjak-Novakovic G, Kaplan DL. Silk fibroin microtubes for blood vessel engineering. *Biomaterials.* 2007;28(35):5271-5279.
17. Lawrence BD, Marchant JK, Pindrus MA, Omenetto FG, Kaplan DL. Silk film biomaterials for cornea tissue engineering. *Biomaterials.* 2009;30(7):1299-1308.
18. Rockwood DN, Preda RC, Yücel T, Wang X, Lovett ML, Kaplan DL. Materials fabrication from Bombyx mori silk fibroin. *Nat Protoc.* 2011;6(10):1612-1631.
19. Lovett ML, Cannizzaro CM, Vunjak-Novakovic G, Kaplan DL. Gel spinning of silk tubes for tissue engineering. *Biomaterials.* 2008;29(35):4650-4657.
20. Cox TR, Erler JT. Remodeling and homeostasis of the extracellular matrix: implications for fibrotic diseases and cancer. *Dis Model Mech.* 2011;4(2):165-178.
21. Malara A, Gruppi C, Pallotta I, et al. Extracellular matrix structure and nano-mechanics determine megakaryocyte function. *Blood.* 2011;118(16):4449-4453.
22. Charras G, Sahai E. Physical influences of the extracellular environment on cell migration. *Nat Rev Mol Cell Biol.* 2014;15(12):813-824.
23. Balduini A, Pallotta I, Malara A, et al. Adhesive receptors, extracellular proteins and myosin IIA orchestrate proplatelet formation by human megakaryocytes. *J Thromb Haemost.* 2008;6(11):1900-1907.
24. Malara A, Gruppi C, Rebuzzini P, et al. Megakaryocyte-matrix interaction within bone marrow: new roles for fibronectin and factor XIII-A. *Blood.* 2011;117(8):2476-2483.
25. Lu Q, Wang X, Hu X, Cebe P, Omenetto F, Kaplan DL. Stabilization and release of enzymes from silk films. *Macromol Biosci.* 2010;10(4):359-368.
26. Gil ES, Panilaitis B, Bellas E, Kaplan DL. Functionalized silk biomaterials for wound healing. *Adv Healthc Mater.* 2013;2(1):206-217.
27. Malara A, Currao M, Gruppi C, et al. Megakaryocytes contribute to the bone marrow-matrix environment by expressing fibronectin, type IV collagen, and laminin. *Stem Cells.* 2014;32(4):926-937.
28. Ingram DA, Mead LE, Tanaka H, et al. Identification of a novel hierarchy of endothelial progenitor cells using human peripheral and umbilical cord blood. *Blood.* 2004;104(9):2752-2760.
29. Thiele W, Krishnan J, Rothley M, et al. VEGFR-3 is expressed on megakaryocyte precursors in the murine bone marrow and plays a regulatory role in megakaryopoiesis. *Blood.* 2012;120(9):1899-1907.
30. Pitchford SC, Lodie T, Rankin SM. VEGFR1 stimulates a CXCR4-dependent translocation of megakaryocytes to the vascular niche, enhancing platelet production in mice. *Blood.* 2012;120(14):2787-2795.
31. Avraham H, Cowley S, Chi SY, Jiang S, Groopman JE. Characterization of adhesive interactions between human endothelial cells and megakaryocytes. *J Clin Invest.* 1993;91(6):2378-2384.
32. Cramer EM, Norol F, Guichard J, et al. Ultrastructure of platelet formation by human megakaryocytes cultured with the Mpl ligand. *Blood.* 1997;89(7):2336-2346.

33. Takayama N, Nishikii H, Usui J, et al. Generation of functional platelets from human embryonic stem cells in vitro via ES-sacs, VEGF-promoted structures that concentrate hematopoietic progenitors. *Blood.* 2008;111(11):5298-5306.

34. Nakamura S, Takayama N, Hirata S, et al. Expandable megakaryocyte cell lines enable clinically applicable generation of platelets from human induced pluripotent stem cells. *Cell Stem Cell.* 2014;14(4):535-548.

35. Mazo IB, von Andrian UH. Adhesion and homing of blood-borne cells in bone marrow microvessels. *J Leukoc Biol.* 1999;66(1):25-32.

36. Jiang J, Woulfe DS, Papoutsakis ET. Shear enhances thrombopoiesis and formation of microparticles that induce megakaryocytic differentiation of stem cells. *Blood.* 2014;124(13): 2094-2103.

37. Mazzucato M, Cozzi MR, Battiston M, et al. Distinct spatio-temporal Ca2+ signaling elicited by integrin alpha2beta1 and glycoprotein VI under flow. *Blood.* 2009;114(13):2793-2801.

38. Mazzucato M, Cozzi MR, Pradella P, Ruggeri ZM, De Marco L. Distinct roles of ADP receptors in von Willebrand factor-mediated platelet signaling and activation under high flow. *Blood.* 2004;104(10): 3221-3227.

39. Ruggeri ZM, Mendolicchio GL. Adhesion mechanisms in platelet function. *Circ Res.* 2007; 100(12):1673-1685.

40. De Cuyper IM, Meinders M, van de Vijver E, et al. A novel flow cytometry-based platelet aggregation assay. *Blood.* 2013;121(10):e70-e80.

41. Tuszynski GP, Kornecki E, Cierniewski C, et al. Association of fibrin with the platelet cytoskeleton. *J Biol Chem.* 1984;259(8):5247-5254.

42. Rooney MM, Parise LV, Lord ST. Dissecting clot retraction and platelet aggregation. Clot retraction does not require an intact fibrinogen gamma chain C terminus. *J Biol Chem.* 1996;271(15): 8553-8555.

43. Borges J, Mueller MC, Padron NT, Tegtmeier F, Lang EM, Stark GB. Engineered adipose tissue supplied by functional microvessels. *Tissue Eng.* 2003;9(6):1263-1270.

44. Wenger A, Stahl A, Weber H, et al. Modulation of in vitro angiogenesis in a three-dimensional spheroidal coculture model for bone tissue engineering. *Tissue Eng.* 2004;10(9-10): 1536-1547.

45. Balduini A, Badalucco S, Pugliano MT, et al. In vitro megakaryocyte differentiation and proplatelet formation in Ph-negative classical myeloproliferative neoplasms: distinct patterns in the different clinical phenotypes. *PLoS ONE.* 2011;6(6):e21015.

46. Shin JW, Swift J, Spinler KR, Discher DE. Myosin-II inhibition and soft 2D matrix maximize multinucleation and cellular projections typical of platelet-producing megakaryocytes. *Proc Natl Acad Sci USA.* 2011;108(28):11458-11463.

47. Feng Q, Chai C, Jiang XS, Leong KW, Mao HQ. Expansion of engrafting human hematopoietic stem/progenitor cells in three-dimensional scaffolds with surface-immobilized fibronectin. *J Biomed Mater Res A.* 2006;78(4):781-791.

48. Dellatore SM, Garcia AS, Miller WM. Mimicking stem cell niches to increase stem cell expansion. *Curr Opin Biotechnol.* 2008;19(5):534-540.

49. Kim DH, Provenzano PP, Smith CL, Levchenko A. Matrix nanotopography as a regulator of cell function. *J Cell Biol.* 2012;197(3):351-360.

50. Zhang J, Pritchard E, Hu X, et al. Stabilization of vaccines and antibiotics in silk and eliminating the cold chain. *Proc Natl Acad Sci USA.* 2012; 109(30):11981-11986.

51. Hamada T, Möhle R, Hesselgesser J, et al. Transendothelial migration of megakaryocytes in response to stromal cell-derived factor 1 (SDF-1) enhances platelet formation. *J Exp Med.* 1998; 188(3):539-548.

52. Magnani M, Rossi L, Bianchi M, et al. Improved stability of 2,3-bisphosphoglycerate during storage of hexokinase-overloaded erythrocytes. *Biotechnol Appl Biochem.* 1989;11(5):439-444.

53. Cabrales P, Tsai AG, Intaglietta M. Modulation of perfusion and oxygenation by red blood cell oxygen affinity during acute anemia. *Am J Respir Cell Mol Biol.* 2008;38(3):354-361.

54. Kaufman RM, Airo R, Pollack S, Crosby WH. Circulating megakaryocytes and platelet release in the lung. *Blood.* 1965;26(6):720-731.

55. Sullenbarger B, Bahng JH, Gruner R, Kotov N, Lasky LC. Prolonged continuous in vitro human platelet production using three-dimensional scaffolds. *Exp Hematol.* 2009; 37(1):101-110.

56. Lasky LC, Sullenbarger B. Manipulation of oxygenation and flow-induced shear stress can increase the in vitro yield of platelets from cord blood. *Tissue Eng Part C Methods.* 2011;17(11): 1081-1088.

57. Schlinker AC, Radwanski K, Wegener C, Min K, Miller WM. Separation of in-vitro-derived megakaryocytes and platelets using spinning-membrane filtration [published online ahead of print October 13, 2014]. *Biotechnol Bioeng.*, doi: 10.1002/bit.25477.

58. Feng Q, Shabrani N, Thon JN, et al. Scalable generation of universal platelets from human induced pluripotent stem cells. *Stem Cell Rev.* 2014;3(5):817-831.

59. Lambert MP, Sullivan SK, Fuentes R, French DL, Poncz M. Challenges and promises for the development of donor-independent platelet transfusions. *Blood.* 2013;121(17):3319-3324.

60. Anitua E, Andia I, Ardanza B, Nurden P, Nurden AT. Autologous platelets as a source of proteins for healing and tissue regeneration. *Thromb Haemost.* 2004;91(1):4-15.